The Journal of Chemical Physics

Full-dimensional automated potential energy surface development and dynamics for the OH + C_2H_6 reaction

Cite as: J. Chem. Phys. **157**, 074307 (2022); https://doi.org/10.1063/5.0104889
Submitted: 21 June 2022 • Accepted: 22 July 2022 • Accepted Manuscript Online: 25 July 2022 • Published Online: 18 August 2022

Balázs Gruber, Viktor Tajti and Gábor Czakó

View Online Export Citation CrossMark

ARTICLES YOU MAY BE INTERESTED IN

Permutation invariant polynomial neural network based diabatic ansatz for the (E + A) × (e + a) Jahn–Teller and Pseudo-Jahn–Teller systems
The Journal of Chemical Physics **157**, 014110 (2022); https://doi.org/10.1063/5.0096912

Photodissociation of quinoline cation: Mapping the potential energy surface
The Journal of Chemical Physics **157**, 064303 (2022); https://doi.org/10.1063/5.0092161

Simplified CCSD(T)-F12 methods: Theory and benchmarks
The Journal of Chemical Physics **130**, 054104 (2009); https://doi.org/10.1063/1.3054300

Lock-in Amplifiers up to 600 MHz
Zurich Instruments
Watch

AIP Publishing

© 2022 Author(s).

The Journal of Chemical Physics ARTICLE scitation.org/journal/jcp

Full-dimensional automated potential energy surface development and dynamics for the OH + C_2H_6 reaction

Cite as: J. Chem. Phys. 157, 074307 (2022); doi: 10.1063/5.0104889
Submitted: 21 June 2022 • Accepted: 22 July 2022 •
Published Online: 18 August 2022

View Online Export Citation CrossMark

Balázs Gruber, Viktor Tajti, and Gábor Czakó[a)]

AFFILIATIONS

MTA-SZTE Lendület Computational Reaction Dynamics Research Group, Interdisciplinary Excellence Centre and Department of Physical Chemistry and Materials Science, Institute of Chemistry, University of Szeged, Rerrich Béla tér 1, Szeged H-6720, Hungary

[a)]Author to whom correspondence should be addressed: gczako@chem.u-szeged.hu

ABSTRACT

We develop a full-dimensional analytical potential energy surface (PES) for the OH + C_2H_6 reaction using the ROBOSURFER program system, which automatically (1) selects geometries from quasi-classical trajectories, (2) performs *ab initio* computations using a coupled-cluster singles, doubles, and perturbative triples-F12/triple-zeta-quality composite method, (3) fits the energies utilizing the permutationally invariant monomial symmetrization approach, and (4) iteratively improves the PES via steps (1)–(3). Quasi-classical trajectory simulations on the new PES reveal that hydrogen abstraction leading to H_2O + C_2H_5 dominates in the collision energy range of 10–50 kcal/mol. The abstraction cross sections increase and the dominant mechanism shifts from rebound (small impact parameters and backward scattering) to stripping (larger impact parameters and forward scattering) with increasing collision energy as opacity functions and scattering angle distributions indicate. The abstraction reaction clearly favors side-on OH attack over O-side and the least-preferred H-side approach, whereas C_2H_6 behaves like a spherical object with only slight C–C-perpendicular side-on preference. The collision energy efficiently flows into the relative translation of the products, whereas product internal energy distributions show only little collision energy dependence. H_2O/C_2H_5 vibrational distributions slightly/significantly violate zero-point energy and are nearly independent of collision energy, whereas the rotational distributions clearly blue-shift as the collision energy increases.

Published under an exclusive license by AIP Publishing. https://doi.org/10.1063/5.0104889

I. INTRODUCTION

Since the accurate theoretical descriptions of three-atom A + BC reactions in the 1970s[1–3] and six-atom processes in the 2000s,[4–11] first-principles high-level *ab initio* potential energy surface (PES)-based dynamics simulations have started to move beyond six-atom systems in the past decade,[12–18] arriving to the nine-atomic atom (H, O, F, Cl) + ethane (C_2H_6)[19–22] and ion + molecule reactions[23–25] around 2020. Full-dimensional quasi-classical trajectory (QCT) simulations as well as full (six-atomic)-[26] and reduced-dimensional quantum dynamics computations for the above mentioned polyatomic reactions shaped our fundamental knowledge on chemical reactivity as well as vibrational and rotational mode specificity.[5–35] In the present work, we aim to push our limits forward by developing a full-dimensional high-level *ab initio* PES for the ten-atomic OH + C_2H_6 reaction, allowing efficient dynamics investigations.

The kinetics of the OH + C_2H_6 → H_2O + C_2H_5 reaction were investigated by early experiments[36,37] and transition-state-theory-based computations.[38] Furthermore, in 2003, Butkovskaya and Setser[39] measured nascent vibrational distributions for the H_2O product via infrared chemiluminescence. Following these early studies, in 2020, two theoretical papers[40,41] appeared on the title reaction in almost coincidence. (1) We reported a benchmark *ab initio* characterization of the stationary points revealing novel hydrogen- and methyl-substitution channels leading to H + C_2H_5OH and CH_3 + CH_3OH, besides the well-known hydrogen-abstraction pathway resulting in H_2O + C_2H_5.[40] (2) Rangel *et al.*[41]

Published under an exclusive license by AIP Publishing

developed a full-dimensional analytical PES for the OH + C_2H_6 → H_2O + C_2H_5 reaction using a valence bond-molecular mechanics (VB-MM) functional form involving 66 adjustable parameters and studied the kinetics and dynamics of the hydrogen-abstraction process.

In the present work, we plan to employ a different approach[42–44] to construct a full-dimensional PES for the OH + C_2H_6 reaction using a flexible permutationally invariant polynomial function of Morse-like variables with 3285 parameters determined by a linear least-squares fit of a large number of high-level *ab initio* energies. The iterative improvement of the PES via sampling the nuclear configurations, *ab initio* computations at the selected geometries, and fitting the *ab initio* data with the monomial symmetrization approach[43] is to be done automatically using the ROBOSURFER program package[45] developed recently in our group. Unlike the VB-MM PES,[41] the new surface will describe all the different product channels and reaction pathways of the OH + C_2H_6 system. Reaction dynamics simulations on the analytical PES will reveal the competitiveness of the hydrogen- and methyl-substitution channels with the main hydrogen-abstraction pathway. Furthermore, we plan to report a detailed dynamical characterization of the title reaction considering cross sections, reaction probabilities, scattering and initial attack angle distributions, as well as product energy distributions and their dependence on collision energy. In Sec. II, we give the details of the PES development and QCT computations; in Sec. III, the results are presented and discussed, and this paper ends with summary and conclusions in Sec. IV.

II. COMPUTATIONAL DETAILS

A. PES development

The PES development begins with generating initial geometries by randomly displacing the Cartesian coordinates of the minima and saddle points in the range of 0–0.32 Å and randomly scattering reactants and products around each other with center of mass distances between 3 and 10 Å while also displacing their Cartesian coordinates in the range of 0–0.20 Å. We use a composite method to compute the energies, in which a basis-set correction is added to the unrestricted explicitly correlated coupled-cluster singles, doubles, and perturbative triples [UCCSD(T)-F12b][46] method utilized with the aug-cc-pVDZ basis set.[47] For the basis-set correction, we use the restricted explicitly correlated second-order Møller–Plesset perturbation theory (RMP2-F12)[48] combined with the aug-cc-pVDZ and aug-cc-pVTZ basis sets, providing high-level composite energies as

$$\begin{aligned} E_{\text{composite}} = {} & \text{UCCSD(T)-F12b/aug-cc-pVDZ} \\ & + (\text{RMP2-F12/aug-cc-pVTZ} \\ & - \text{RMP2-F12/aug-cc-pVDZ}). \end{aligned} \tag{1}$$

All the *ab initio* computations are performed using the MOLPRO program package.[49]

From the initial dataset, the PES development is carried out using the ROBOSURFER program system,[45] which was recently developed in our research group. New geometries are added between −30 and 150 kcal/mol relative to the reactants. The development starts with 2393 composite energy points. The fitting of the energy points is executed within the framework of the monomial symmetrization approach (MSA)[43] of the permutationally invariant polynomial method.[42,44] We use a full-dimensional analytical Morse-like function that is invariant under the permutation of like atoms. This function is constructed as an expansion of polynomials of $y_{ij} = \exp(-r_{ij}/a)$, where r_{ij} are the atom–atom distances and the a parameter controls the asymptotic behavior of the PES. In this study, we choose the a parameter as 2 bohrs. At the beginning of the development, the polynomial order is 4 because the initial PES contains less energy points than the number of the coefficients in a fifth-order fit. The fourth-order expansion requires 715 coefficients, and the fifth-order includes 3285 coefficients. The coefficients are determined using a weighted linear least-squares fit to the *ab initio* data applying a weight function of $E_0/(E + E_0)$, where E is the potential energy relative to the minimum of the dataset and E_0 is set to 0.05 E_h (31.4 kcal/mol). New geometries are added to improve the PES from QCT computations, where the b impact parameter is chosen as 0, 0.5, 1.0, 1.5, and 2.0 bohrs. The development starts with 10 kcal/mol collision energy (E_{coll}), and when the quality of the PES is sufficient, we increase E_{coll} by 10 kcal/mol. The maximum of E_{coll} is 60 kcal/mol during the development. The quality of the PES is assessed by the number of unphysical trajectories and one-dimensional scans along representative inter-molecular coordinates. After 1946 iterations, we continue to develop from the H_2O + C_2H_5 direction at 30 kcal/mol collision energy to improve the PES even more. 18 iterations are performed in this backward direction, while 458 energy points are added. The final PES contains 12 544 geometries, and the root-mean-square (rms) error is quite small in the chemically interesting energy ranges. In the 0.0–31.4 kcal/mol region relative to the global minimum of the PES, the rms error is 0.63 kcal/mol, and in the 31.4–62.8 kcal/mol region, the rms value is 0.87 kcal/mol. Moreover, the overall rms fitting error is 0.83 kcal/mol, which is also within the chemical accuracy.

B. Quasi-classical trajectory simulations

Quasi-classical dynamics simulations are performed at collision energies of 10, 20, 30, 40, and 50 kcal/mol for the OH(v = 0) + C_2H_6(v = 0) reaction. The zero-point energies (ZPEs) of the reactants are set at the beginning of the trajectories using normal-mode sampling.[50] The orientations of the reactants are randomly rotated. The initial distance of the center of masses of the reactants is $\sqrt{x^2 + b^2}$, where x = 18.90 bohrs (10 Å) and the b impact parameter is varied between 0 and 8 bohrs with 0.5 bohr steps. We run 1000 trajectories at every variation of collision energy and impact parameter, which means 85 000 simulations altogether. Integral cross sections (σ) are calculated using numerical integration,

$$\sigma = \pi \sum_{n=1}^{n_{\max}} [b_n - b_{n-1}][b_n P(b_n) + b_{n-1} P(b_{n-1})], \tag{2}$$

where $P(b)$ is the opacity function and $n_{\max}$ is the number of parts we divide the range $[0, b_{\max}]$. $b_{\max}$ is the maximum impact parameter where reactive trajectories can be noticed. In the present study, $b_n = 0.5n$ bohr, where $n = 0, 1, \ldots, n_{\max}$. We use two kinds of ZPE

Published under an exclusive license by AIP Publishing

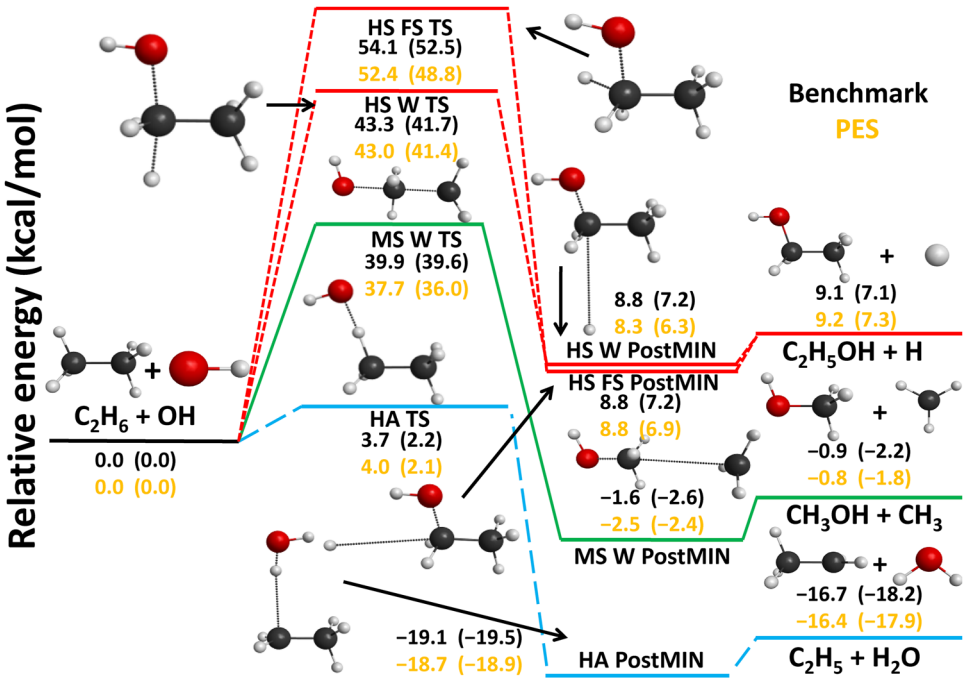

FIG. 1. Schematic potential energy surface of the OH + C_2H_6 reaction showing the structures and classical (adiabatic) relative energies of the stationary points along the different reaction pathways. The relativistic all-electron CCSDT(Q)/complete-basis-set-quality benchmark relative energies are taken from Ref. 40, and the PES values are obtained on the present PES.

constraints for the products: soft and hard. In the soft case, those trajectories are not considered as reactive when the sum of the classical vibrational energy of the C_2H_5 radical and that of the H_2O molecule is smaller than the sum of their harmonic ZPEs. Within the hard constraint, each classical vibrational energy of the different chemical species must be larger separately than the corresponding harmonic ZPE on the PES. The scattering angle distributions are determined by binning the cosine of the angle (θ) of the relative velocity vectors of the center of masses of the products and reactants into ten equidistant bins from −1 to 1. $\cos(\theta) = -1(\theta = 180^\circ)$ means backward scattering, and $\cos(\theta) = 1(\theta = 0^\circ)$ corresponds to forward scattering. Furthermore, we calculate the attack angle distributions for the reactants by binning the cosine of the angle (α) of the velocity vector of the center of mass of the examined reactant and an interatomic vector, which is considered as the O–H bond for the hydroxil radical and the C–C bond for the ethane molecule. We also use ten equidistant bins between −1 and 1 like in the case of scattering angle distributions. $\cos(\alpha) = -1$ means that the OH radical approaches the ethane molecule with its O-atom side, and in the situation of $\cos(\alpha) = 1$, the OH radical goes with its H atom toward the ethane molecule. Rotational quantum numbers of the H_2O and C_2H_5 products are obtained by rounding the lengths of classical rotational angular momentum vectors to the nearest integer values.

III. RESULTS AND DISCUSSION

The potential energy diagram of the OH + C_2H_6 reaction showing the different pathways and the comparison of the stationary-point relative energies obtained on the analytical PES with relativistic all-electron coupled-cluster singles, doubles, triples, and perturbative quadruples [CCSDT(Q)]/complete-basis-set-quality benchmark values[40] is presented in Fig. 1. The H-abstraction channel leading to H_2O + C_2H_5 is exothermic, $\Delta E_e(\Delta H_0) = -16.4$ (−17.9) kcal/mol, and has a small classical(adiabatic) barrier of 4.0(2.1) kcal/mol on the PES. The above relative energy values agree with the benchmark data[40] within 0.1–0.3 kcal/mol, showing the high accuracy of the PES. The methyl-substitution channel resulting in CH_3 + CH_3OH is slightly exothermic, $\Delta E_e(\Delta H_0) = -0.8$ (−1.8) kcal/mol, whereas the H-substitution forming H + C_2H_5OH is endothermic, $\Delta E_e(\Delta H_0) = 9.2(7.3)$ kcal/mol. Based on thermodynamics, these channels can open at low collision energies; however, they are kinetically hindered because they have significant Walden-inversion (W) barrier heights of 37.7(36.0) and 43.0

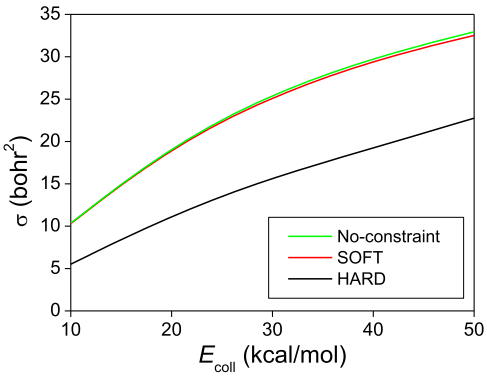

FIG. 2. Cross sections of the OH + $C_2H_6 \rightarrow H_2O + C_2H_5$ reaction as a function of collision energy obtained without as well as with soft and hard ZPE constraints.

Published under an exclusive license by AIP Publishing

(41.4) kcal/mol, respectively. In the case of H substitution, a front-side attack transition state (HS FS TS) is also found, but the corresponding barrier height of 52.4(48.8) kcal/mol is higher than that of the Walden-inversion pathway. The reaction enthalpies for methyl- and H-substitution agree very well with the benchmark data; the largest deviation is only 0.4 kcal/mol, as seen in Fig. 1. The high-energy transition states are less accurate on the PES, except the fortuitous accuracy of HS W TS, due to their less frequent sampling and lower weight during the fitting. We do not consider this a serious issue because the main interest is in the H-abstraction channel as we discuss below in more detail.

QCT simulations reveal that in the collision energy range of the present study (10–50 kcal/mol), the H-abstraction channel dominates with cross sections in the 10–33 bohrs^2 range; the methyl- and H-substitution channels open around 30–40 kcal/mol, but their cross sections are only 0.02 and 0.03 bohr^2 at E_{coll} = 50 kcal/mol, respectively. We may expect increasing reactivity of these substitution channels at higher collision energies; however, the present PES development only ensures high accuracy up to E_{coll} of 50 kcal/mol; therefore, in this study, we do not consider these channels further, but we focus on the major H-abstraction reaction.

Figure 2 shows the cross sections for the H-abstraction channel as a function of collision energy. The cross sections increase with the increasing collision energy, and the excitation function has a similar shape as that of the F + C_2H_6 reaction;[21] however, the reactivity of OH + C_2H_6 is less by about a factor of 3. The similarity of the two isoelectronic reactions is expected because both are exothermic with low, early (reactant-like) barriers. The lower reactivity of OH + C_2H_6 relative to that of F + C_2H_6 may be explained by the slightly higher barrier of the former, the two-times higher exothermicity of the latter which hinders re-crossing, and, perhaps most importantly, by the fact that unlike the F atom, the OH radical may need a special orientation to abstract an H atom. This last statement will be investigated in more detail below. Figure 2 also shows that the soft ZPE constraint has virtually no effect on the cross sections, similar to the case of F + C_2H_6,[21] whereas the hard constraint decreases the reactivity by factors of 1.88, 1.73, 1.63, 1.56, and 1.45 at E_{coll} = 10, 20, 30, 40, and 50 kcal/mol, respectively. The relatively slight collision energy dependence of the ZPE violation effects suggests that there is no substantial energy transfer between the initial translational energy and the final vibrational states or the energy transfer does not significantly depend on E_{coll} (see more details below).

Opacity functions (reaction probabilities as a function of impact parameter) and scattering angle distributions are shown in Figs. 3 and 4, respectively. The maximum impact parameter is around 6.5 bohrs without any significant E_{coll} dependence. At b = 0, the reactivity first increases with increasing E_{coll}, as the reaction probabilities are 18%, 33%, and 40% at E_{coll} = 10, 20, and 30 kcal/mol, respectively. However, in the 30–50 kcal/mol E_{coll} range, the b = 0 reaction probability is around 40%–44% without significant E_{coll} dependence. Thus, the increasing cross sections can be explained by the change of the shape of the opacity functions, i.e., at low E_{coll}, the reaction probabilities decrease monotonically with increasing b, whereas at highest E_{coll}, the probabilities are nearly constant up to b = 4 bohrs and then decay rapidly. The preference of larger impact parameters increases with increasing E_{coll}. This indicates that the rebound mechanism, occurring at small b,

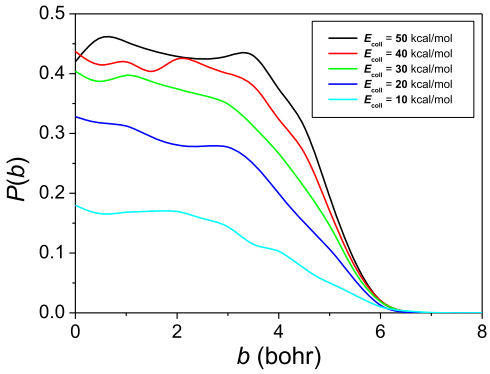

FIG. 3. Reaction probabilities of the OH + C_2H_6 → H_2O + C_2H_5 reaction as a function of impact parameter at different collision energies obtained without the ZPE constraint.

dominates at low E_{coll}, and the probability of direct stripping, favoring larger b values, increases with increasing E_{coll}. These findings are in accord with the shapes of the scattering angle distributions (Fig. 4). At the lowest E_{coll}, backward scattering dominates as a signature of direct rebound, and as E_{coll} increases, the forward direction becomes more and more pronounced, and at the highest collision energies, forward scattering is clearly favored, indicating the dominance of the direct stripping mechanism. The distributions also have some isotropic feature, especially at low E_{coll}, indicating significant complex-forming, indirect dynamics as well.

Initial attack angle distributions are shown in Fig. 5. The distributions show that O-side attack of the OH radical is preferred over H-side attack, as expected, because an O–H bond forms in the abstraction process. However, this O-side attack preference is not significant, and somewhat unexpectedly, side-on attack of the OH radical is clearly preferred relative to the O-side and H-side attacks since the distributions peak at α = 90°, especially at low E_{coll}. Examining the HA TS structure (Fig. 1), one can see that the H–O–H angle at the TS is also close to 90°; thus, the side-on attack

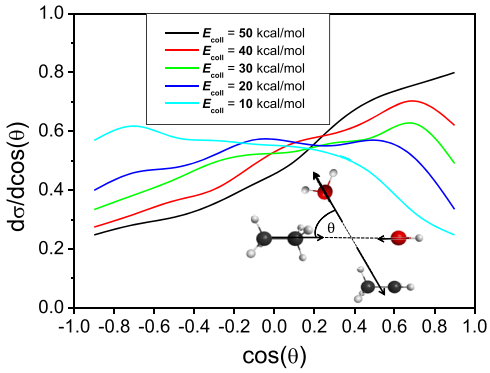

FIG. 4. Normalized scattering angle distributions for the OH + C_2H_6 → H_2O + C_2H_5 reaction at different collision energies obtained without the ZPE constraint.

Published under an exclusive license by AIP Publishing

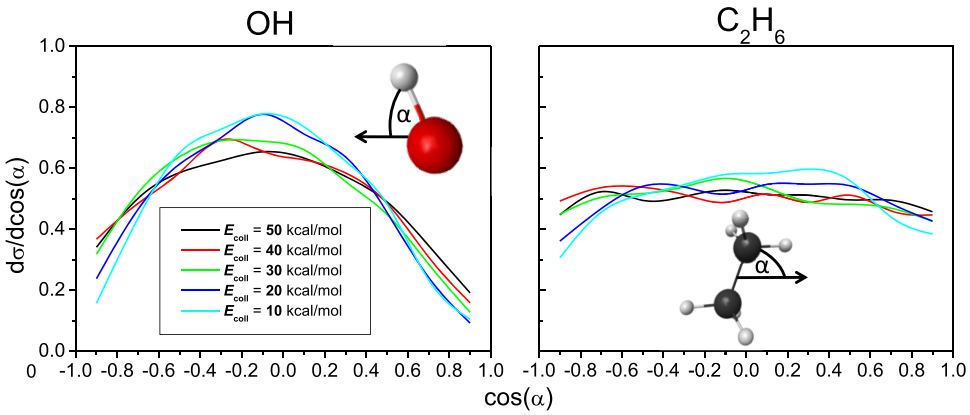

FIG. 5. Normalized initial attack angle distributions for the OH + C_2H_6 → H_2O + C_2H_5 reaction at different collision energies obtained without the ZPE constraint. The attack angles are defined at the beginning of each reactive trajectory as shown in the pictograms.

is preferred if OH approaches C_2H_6 perpendicular to the C–C bond. Looking at the attack angle distributions of the C_2H_6 reactant, a slight preference of the side-on (perpendicular) attack is seen indeed, especially at low E_{coll}, in accord with the above findings. However, as E_{coll} increases, the C_2H_6 attack angle distributions become nearly isotropic, showing that the C_2H_6 molecule almost behaves as a spherical object, like CH_4. Note that due to the symmetry of C_2H_6, its attack angle distributions should be exactly back-side–front-side symmetric, which is seen in the right panel of Fig. 5 within statistical accuracy.

Figure 6 shows the relative translational energy distributions of the H_2O and C_2H_5 products of the OH + C_2H_6 reaction. As seen, the distributions shift toward higher translational energies and become broader as E_{coll} increases, and these shifts correspond to the increment of the collision energy showing efficient translational energy transfer between the reactants and products. Considering the shape of the distributions, one can observe that at the lowest E_{coll}, the distribution peaks at a lower translational energy and the peaks shift toward the highest available translational energies as E_{coll} increases. This finding indicates that the reaction becomes more and more direct as E_{coll} increases, in accord with the scattering angle distributions.

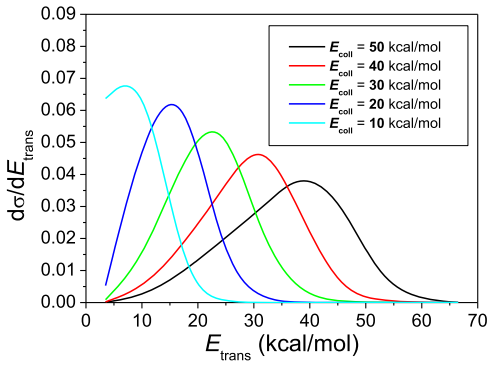

FIG. 6. Normalized product relative translational energy distributions for the OH + C_2H_6 → H_2O + C_2H_5 reaction at different collision energies obtained without the ZPE constraint.

Internal energy distributions for the H_2O and C_2H_5 products as well as their decompositions into vibrational and rotational counterparts are shown in Fig. 7. The internal energy distributions of H_2O are clearly hotter, relative to ZPE, with only slight ZPE violation than those of the C_2H_5 co-product, where the ZPE violation is significant. The finding that the OH + C_2H_6 reaction produces vibrationally excited H_2O molecules is in accord with the elongated O–H distance at the reactant-like transition state. The distributions become only slightly broader, and their peaks blue-shift by only a few kcal/mol as E_{coll} increases from 10 to 50 kcal/mol, showing only little collision energy transfer to the product internal degrees of freedom. Moreover, the H_2O vibrational energy distributions, which are slightly colder than the corresponding internal energy ones, show even less and somewhat inverse E_{coll} dependence. The rotational energy distributions of the H_2O product, however, become clearly hotter as E_{coll} increases; thus, the slight blue-shifting E_{coll} dependence of the H_2O internal energy distributions originates from translational-rotational energy transfer. In the case of the C_2H_5 product, the rotational energy distributions are slightly hotter and have similar E_{coll} dependence than those of H_2O; thus, the C_2H_5 vibrational energy distributions are even colder and show less E_{coll} dependence than the internal energy ones. These findings are consistent with the effects of the ZPE constraints on the cross sections. The vibrational excitation of the H_2O product can compensate the ZPE violation of C_2H_5, and in some cases, the reverse is true; therefore, the soft constraint does not affect the cross sections. In the case of the hard constraint, mostly the significant ZPE violation of C_2H_5 and, to a lesser extent, that of H_2O decrease the cross sections by nearly a constant factor within 1.45–1.88 as the H_2O and C_2H_5 vibrational distributions only slightly depend on E_{coll}. Figure 7 also shows rotational quantum number (J) value distributions of the products. The J distributions of both H_2O and C_2H_5 become broader and hotter as E_{coll} increases, in accord with the rotational energy distributions. Finally, we note that the J distributions of H_2O span a significantly smaller range (0–30) than those of C_2H_5 (0–120) even if the rotational energies are only slightly colder for H_2O, which is due to the much larger moments of inertia of C_2H_5 than those of H_2O.

Published under an exclusive license by AIP Publishing

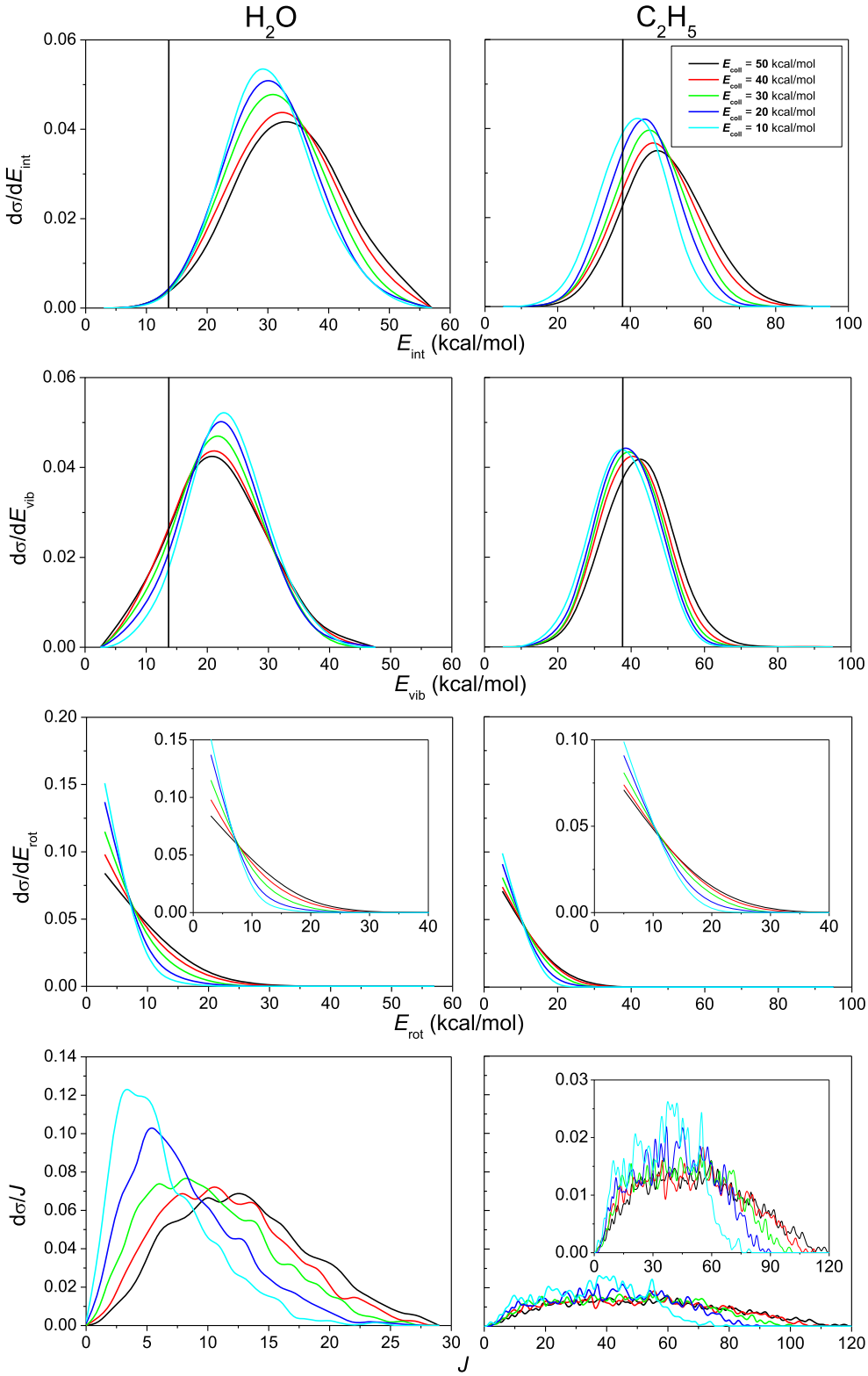

FIG. 7. Normalized internal energy (E_{int}), vibrational energy (E_{vib}), rotational energy (E_{rot}), and rotational quantum number (J) value distributions for the H_2O and C_2H_5 products of the OH + C_2H_6 reaction at different collision energies obtained without the ZPE constraint. Vertical lines indicate the ZPEs of the products.

Published under an exclusive license by AIP Publishing

IV. SUMMARY AND CONCLUSIONS

Following our recent studies on analytical PES developments for nine-atomic reactive systems, such as F/Cl + C_2H_6[21,22] and F^- + CH_3CH_2Cl,[24] in the present work, we have reported a high-level full-dimensional *ab initio* PES for the ten-atomic OH + C_2H_6 reaction. The PES has been automatically constructed using the ROBOSURFER program system,[45] interfaced to the monomial symmetrization approach (MSA) fitting code[43] and the MOLPRO *ab initio* program package.[49] The PES describes the H-abstraction, methyl-substitution, and H-substitution channels of the title reaction; however, QCT computations reveal that the substitution reactivity is negligible in the collision energy range of 10–50 kcal/mol; therefore, in the present study, we have focused on the H-abstraction channel leading to the H_2O + C_2H_5 products. The results of the dynamics simulations can be summarized as follows:

(a) The cross sections of the H-abstraction process increase with increasing collision energy, similar to the F + C_2H_6 reaction.[21] The soft ZPE constraint does not affect the reactivity, whereas the hard constraint decreases the cross sections by a factor of around 1.88–1.45 in the 10–50 kcal/mol collision energy range.

(b) The maximum impact parameters do not have significant collision energy dependence, but the shape of the opacity functions changes with E_{coll} favoring higher and higher impact parameters as E_{coll} increases. This is consistent with the scattering angle distributions showing a shift from backward to forward dominance as E_{coll} increases. These findings indicate that at low E_{coll}, the reaction prefers the direct rebound pathway, whereas at higher E_{coll}, direct stripping becomes the main reaction pathway.

(c) Initial attack angle distributions reveal significant and slight side-on collision preferences for OH and C_2H_6, respectively, especially at low collision energies. As expected, the O-side attack is preferred over the H-side attack for OH; however, somewhat unexpectedly, the side-on attack is two to four-times more reactive than the O-side attack.

(d) Product relative translational energy distributions show efficient energy transfer between the reactant and product translational modes, whereas the product internal energy distributions show only slight collision energy dependence. Furthermore, we have found that the vibrational energy distributions of the H_2O and C_2H_5 products are even less dependent on collision energy, in accord with the nearly constant relative effect of the hard ZPE constraint, whereas their rotational counterparts clearly blue-shift as E_{coll} increases. The ZPE violation is less significant for H_2O because of the early barrier nature of the hydrogen-abstraction process. The slightly hotter rotational energy distributions of C_2H_5 correspond to significantly higher J excitations than those of H_2O due to the larger moments of inertia of the former product.

The present PES opens the door for several dynamics studies, such as (a) reduced-dimensional quantum wave-packet computations, which may be important at low collision energies where tunneling can be significant, (b) vibrational and rotational mode-specific simulations, (c) determination of mode-specific product vibrational distributions allowing comparison with experiment,[39] and (d) investigation of the isotope effect on the dynamics and/or kinetics. Furthermore, our study may motivate crossed-beam experiments for the title reaction and further improvement of the high-energy region of the PES, where the substitution channels open and may compete with the abstraction process at hyperthermal collision energies.

SUPPLEMENTARY MATERIAL

See the supplementary material for codes[43] and coefficients for the evaluation of the potential energy surface.

ACKNOWLEDGMENTS

We acknowledge the National Research, Development and Innovation Office—NKFIH (Grant No. K-125317); the Ministry of Human Capacities, Hungary (Grant No. 20391-3/2018/FEKUSTRAT); Project No. TKP2021-NVA-19, provided by the Ministry of Innovation and Technology of Hungary from the National Research, Development and Innovation Fund, financed under the TKP2021-NVA funding scheme; and the Momentum (Lendület) Program of the Hungarian Academy of Sciences for the financial support.

AUTHOR DECLARATIONS

Conflict of Interest

The authors have no conflicts to disclose.

Author Contributions

Balázs Gruber: Data curation (lead); Formal analysis (lead); Investigation (lead); Methodology (equal); Validation (equal); Visualization (lead); Writing – original draft (supporting); Writing – review & editing (supporting). **Viktor Tajti**: Data curation (supporting); Formal analysis (supporting); Investigation (supporting); Methodology (equal); Software (lead); Supervision (supporting); Validation (equal); Visualization (supporting). **Gábor Czakó**: Conceptualization (lead); Funding acquisition (lead); Investigation (supporting); Methodology (supporting); Project administration (lead); Resources (lead); Software (supporting); Supervision (lead); Validation (equal); Visualization (supporting); Writing – original draft (lead); Writing – review & editing (lead).

DATA AVAILABILITY

The data that support the findings of this study are available from the corresponding author upon reasonable request.

REFERENCES

[1] G. C. Schatz and A. Kuppermann, J. Chem. Phys. **62**, 2502 (1975).
[2] G. C. Schatz and A. Kuppermann, J. Chem. Phys. **65**, 4642 (1976).
[3] A. Persky, J. Chem. Phys. **66**, 2932 (1977).
[4] M. A. Collins, Theor. Chem. Acc. **108**, 313 (2002).
[5] J. F. Castillo, F. J. Aoiz, L. Bañares, E. Martinez-Nuñez, A. Fernández-Ramos, and S. Vazquez, J. Phys. Chem. A **109**, 8459 (2005).

Published under an exclusive license by AIP Publishing

[6]Z. Xie, J. M. Bowman, and X. Zhang, J. Chem. Phys. **125**, 133120 (2006).
[7]J. F. Castillo, F. J. Aoiz, and L. Bañares, J. Chem. Phys. **125**, 124316 (2006).
[8]M. Yang, S.-Y. Lee, and D. H. Zhang, J. Chem. Phys. **126**, 064303 (2007).
[9]J. Espinosa-García, J. L. Bravo, and C. Rangel, J. Phys. Chem. A **111**, 2761 (2007).
[10]G. Czakó, B. C. Shepler, B. J. Braams, and J. M. Bowman, J. Chem. Phys. **130**, 084301 (2009).
[11]G. Czakó and J. M. Bowman, Science **334**, 343 (2011).
[12]B. Fu, Y.-C. Han, J. M. Bowman, L. Angelucci, N. Balucani, F. Leonori, and P. Casavecchia, Proc. Natl. Acad. Sci. U. S. A. **109**, 9733 (2012).
[13]J. Li and H. Guo, J. Chem. Phys. **143**, 221103 (2015).
[14]M. L. Weichman, J. A. DeVine, M. C. Babin, J. Li, L. Guo, J. Ma, H. Guo, and D. M. Neumark, Nat. Chem. **9**, 950 (2017).
[15]O. Roncero, A. Zanchet, and A. Aguado, Phys. Chem. Chem. Phys. **20**, 25951 (2018).
[16]D. Lu, J. Behler, and J. Li, J. Phys. Chem. A **124**, 5737 (2020).
[17]D. Lu, J. Li, and H. Guo, CCS Chem. **2**, 882 (2020).
[18]D. A. Tasi, T. Győri, and G. Czakó, Phys. Chem. Chem. Phys. **22**, 3775 (2020).
[19]J. Espinosa-Garcia, M. Garcia-Chamorro, and J. C. Corchado, Phys. Chem. Chem. Phys. **21**, 13347 (2019).
[20]J. Espinosa-Garcia, C. Rangel, J. C. Corchado, and M. Garcia-Chamorro, Phys. Chem. Chem. Phys. **22**, 22591 (2020).
[21]D. Papp and G. Czakó, J. Chem. Phys. **153**, 064305 (2020).
[22]D. Papp, V. Tajti, T. Győri, and G. Czakó, J. Phys. Chem. Lett. **11**, 4762 (2020).
[23]B. Bastian, T. Michaelsen, L. Li, M. Ončák, J. Meyer, D. H. Zhang, and R. Wester, J. Phys. Chem. A **124**, 1929 (2020).
[24]J. Meyer, V. Tajti, E. Carrascosa, T. Győri, M. Stei, T. Michaelsen, B. Bastian, G. Czakó, and R. Wester, Nat. Chem. **13**, 977 (2021).
[25]X. Lu, L. Li, X. Zhang, B. Fu, X. Xu, and D. H. Zhang, J. Phys. Chem. Lett. **13**, 5253 (2022).
[26]R. Welsch and U. Manthe, J. Chem. Phys. **138**, 164118 (2013).
[27]F. Meng, W. Yan, and D. Wang, Phys. Chem. Chem. Phys. **14**, 13656 (2012).
[28]R. Liu, F. Wang, B. Jiang, G. Czakó, M. Yang, K. Liu, and H. Guo, J. Chem. Phys. **141**, 074310 (2014).
[29]B. Fu, X. Shan, D. H. Zhang, and D. C. Clary, Chem. Soc. Rev. **46**, 7625 (2017).
[30]N. Liu and M. Yang, J. Chem. Phys. **143**, 134305 (2015).
[31]H. Song, J. Li, B. Jiang, M. Yang, Y. Lu, and H. Guo, J. Chem. Phys. **140**, 084307 (2014).
[32]D. Papp, J. Li, H. Guo, and G. Czakó, J. Chem. Phys. **155**, 114303 (2021).
[33]D. Papp and G. Czakó, J. Chem. Phys. **155**, 154302 (2021).
[34]D. Papp and G. Czakó, J. Phys. Chem. A **126**, 2551 (2022).
[35]D. Gao and D. Wang, Phys. Chem. Chem. Phys. **23**, 26911 (2021).
[36]D. L. Baulch, R. J. B. Craven, M. Din, D. D. Drysdale, S. Grant, D. J. Richardson, A. Walker, and G. Watling, J. Chem. Soc., Faraday Trans. 1 **79**, 689 (1983).
[37]F. P. Tully, A. T. Droege, M. L. Koszykowski, and C. F. Melius, J. Phys. Chem. **90**, 691 (1986).
[38]J. P. Senosiain, C. B. Musgrave, and D. M. Golden, J. Phys. Chem. A **105**, 1669 (2001).
[39]N. I. Butkovskaya and D. W. Setser, Int. Rev. Phys. Chem. **22**, 1 (2003).
[40]B. Gruber and G. Czakó, Phys. Chem. Chem. Phys. **22**, 14560 (2020).
[41]C. Rangel, M. Garcia-Chamorro, J. C. Corchado, and J. Espinosa-Garcia, Phys. Chem. Chem. Phys. **22**, 14796 (2020).
[42]B. J. Braams and J. M. Bowman, Int. Rev. Phys. Chem. **28**, 577 (2009).
[43]Z. Xie and J. M. Bowman, J. Chem. Theory Comput. **6**, 26 (2010).
[44]J. M. Bowman, G. Czakó, and B. Fu, Phys. Chem. Chem. Phys. **13**, 8094 (2011).
[45]T. Győri and G. Czakó, J. Chem. Theory Comput. **16**, 51 (2020).
[46]G. Knizia, T. B. Adler, and H.-J. Werner, J. Chem. Phys. **130**, 054104 (2009).
[47]T. H. Dunning, Jr., J. Chem. Phys. **90**, 1007 (1989).
[48]G. Knizia and H.-J. Werner, J. Chem. Phys. **128**, 154103 (2008).
[49]H.-J. Werner, P. J. Knowles, G. Knizia, F. R. Manby, M. Schütz *et al.*, MOLPRO, version 2015.1, a package of *ab initio* programs, 2015, see http://www.molpro.net.
[50]W. L. Hase, *Encyclopedia of Computational Chemistry* (Wiley, New York, 1998), pp. 399–407.

Published under an exclusive license by AIP Publishing